European Journal of Control (2011)3:290–301

DOI:10.3166/EJC.17.290–301

European Journal of Control

Controller Design for a High-Sampling-Rate Closed-Loop Adaptive Optics System with Piezo-Driven Deformable Mirror

Hong Song[1,*], Rufus Fraanje[1], Georg Schitter[2], Gleb Vdovin[3], Michel Verhaegen[1]

[1] Delft Center for Systems and Control, Delft University of Technology, Delft, The Netherlands;
[2] Automation and Control Institute, Vienna University of Technology, Vienna, Austria;
[3] Flexible Optical B.V., Polakweg 10, Rijswijk, The Netherlands

Adaptive Optics (AO) systems are widely used in many scientific and medical applications, such as astronomy, laser systems and microscopes, in order to improve the resolution of the image by actively sensing and compensating the optical aberration in the system. This paper aims at improving the performance of a closed-loop AO system with Piezo-driven Deformable Mirror (PDM) and high-sampling-rate Wavefront Sensor (WFS) by means of model-based control. The improvement is achieved by reducing the hysteresis in the PDM with a hysteresis compensator and identifying a linear dynamic model of the AO system from the measurement data with a closed-loop subspace identification approach. Based on the identified model of the AO system and the model of the disturbance, a dynamic controller is designed. Experimental results show that the variance of the residual error of the proposed closed-loop AO system has been reduced by 30% with respect to the conventional AO control approach.

Keywords: Adaptive optics, hysteresis compensation, closed-loop subspace identification, model-based controller design

1. Introduction

The resolution of many optical imaging systems, like telescopes, microscopes, is limited by the diffraction of light [3]. However, in most practical cases, the optical aberration in the light path is the dominant limitation of the resolution of the imaging system. Therefore adaptive optics (AO) systems have been widely used in many scientific and medical applications, such as astronomy, laser systems and microscopes, to improve the image quality, by actively sensing and compensating the optical aberration in the system [31, 34].

Conventional closed-loop AO controllers [31, 34] consists of a linear static gain, the pseudo-inverse of the deformable mirror (DM) influence matrix, and an integrator. The gain is tuned to make a trade-off among disturbance rejection, noise amplification and closed-loop stability [12, 16]. To further improve the performance of the closed-loop AO system, controllers based on both the deterministic AO model and the stochastic model of the disturbance have been proposed [20, 24, 25, 28, 29, 32]. Performance improvement of such closed-loop AO systems have been demonstrated in laboratory experiments by [20] and [29], at a closed-loop sampling rate of 25 Hz and 60 Hz, respectively. As the sampling rate increases in modern AO systems [22], the dynamics of the AO system becomes more significant and an accurate dynamic model of the AO system is important for model-based controller design. Looze [25] built a dynamic model of the AO system based on the dynamic models of the DM and the wavefront sensor (WFS), and evaluated the performance improvement of the closed-loop AO system by simulation. Chiuso *et al.* [5] applied a closed-loop subspace identification approach for the AO system based

Correspondence to: H. Song, E-mail: H.Song@tudelft.nl

Received 2 December 2009; Accepted 14 October 2010
Recommended by C. Kulcsár, H.-F. Raynaud, J.-M. Conan, D.W. Clarke

on the measurement data. Because the identification process is based on real data without assumption on the timing of the AO system, the accuracy of the AO model is improved.

In this paper we continue the line of improving the performance of a closed-loop AO system with nonlinear piezo-driven DM (PDM) and high-sampling-rate WFS by means of model-based control. Apart from PDMs, bimorph DMs [11, 23, 37], electromagnetic DMs [15, 18] and DMs based on microelectromechanical systems (MEMS) technology [1, 2, 35] have also been used or proposed in many closed-loop AO systems. A PDM is considered in our work because PDMs are able to provide large amplitude wavefront manipulation required by atmospheric disturbance rejection and have been widely used [8, 13, 22, 33]. Furthermore, the nonlinearity in the PDM (e.g. the hysteresis) makes the controller design even more challenging in large-amplitude-disturbance rejection. By demonstrating controller design for a PDM, our controller design strategy is also applicable to other types of DMs.

The main contribution of this paper is to make high performance AO control design accessible to the new developments in control relevant modeling and identification [5, 17]. This is reflected in two aspects: (1) nonlinearity in the PDM is modeled and compensated, enabling the use of existing linear system identification and controller design approach for control of high-sampling-rate closed-loop AO system; (2) the controller and the model are validated by evaluating the performance of the closed-loop AO system in the experimental setup. The investigation is carried as follows. First, the hysteresis in the PDM is reduced by a hysteresis compensator using feedforward control [11, 37]. By doing this, the linearity of the AO system is improved even in case of large-amplitude control signal. Second, a linear dynamic model of the AO system is identified using a closed-loop subspace identification approach [5]. Because the experimental condition for identification is close to that for closed-loop operation, a realistic model of the AO system is identified for controller design [17]. Third, a dynamic controller is designed based on the identified model of the AO system and a disturbance model. Fourth, the performance of the closed-loop AO system with the proposed controller is evaluated experimentally. Comparison is also made in closed-loop performance between the proposed controller and the conventional controller.

The paper is organized as follows. Section 2 gives the description of the system. Section 3 focuses on identification of the AO system for controller design. Section 4 designs the model-based controller. Section 5 reports and evaluates the experimental results on identification of the AO system and the performance of the closed-loop AO system. Section 6 concludes the work.

2. System Description

The schematic of the common closed-loop AO system [31, 34] under investigation is shown in Fig. 1 (left). The collimated laser beam passes through the beam splitter (BS) first, then reflected by the DM and directed to the Shack-Hartmann (S-H) WFS. The S-H WFS transfers the local gradients of the incident wavefront to the spot displacements in the imaging plane of the CCD camera, denoted as $y(k) \in \mathbb{R}^{m_y}$ with m_y the number of measurements at time instant k. The disturbance, denoted as $d(k) \in \mathbb{R}^{m_y}$, is introduced numerically in the computer after the measurement. $d(k)$ is generated by $d(k) = D(z)s(k)$, where $s(k) \in \mathbb{R}^{m_s}$ (m_s is the dimension of $s(k)$) is a white and stationary random process with zero-mean and unit covariance and $D(z)$ a dynamic filter producing colored noise. Based on the residual error $e(k) = d(k) - y(k)$, the voltages $V(k) \in \mathbb{R}^{m_u}$ (m_u is the number of actuators)

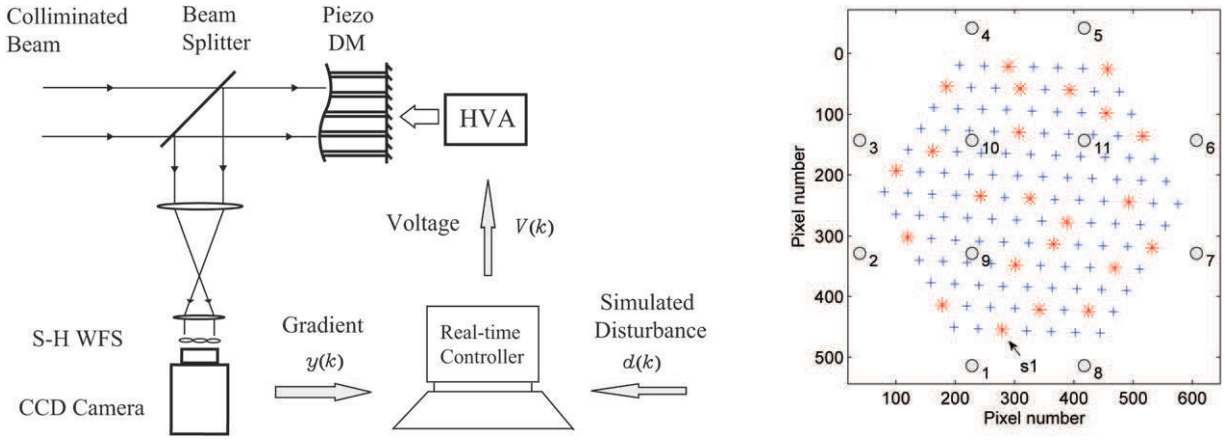

Fig. 1. Left: schematic of the closed-loop AO system; right: layout of the actuator (∘) and the S-H WFS (+) in the imaging plane of the CCD camera.

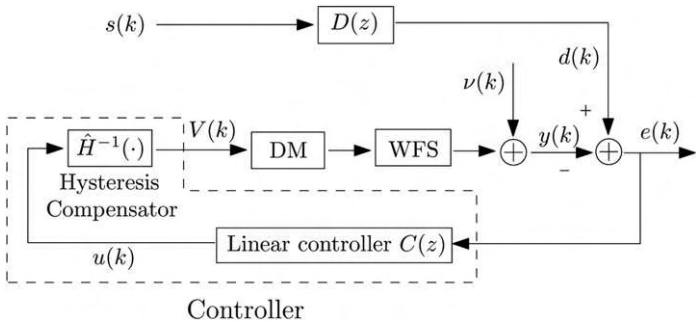

Fig. 2. Block diagram of the closed-loop AO system, with $\nu(k)$ the measurement noise.

are generated by the controller to drive the DM such that the disturbance is rejected. As is discussed in Section 3, since hysteresis occurs at the input of the DM, a hysteresis compensator $\hat{H}^{-1}(\cdot)$ is placed before the DM to reduce the hysteresis and a linear controller $C(z)$ is designed to take care of the linear part of the AO system (see Fig. 2).

In the experimental setup, the DM prototype (OKOTech, Delft, The Netherlands) has a clear aperture of 25 mm and the mirror plate is supported by 11 piezoelectric tubes (PT130.00, Physik Instrumente, Germany). The piezo actuators are driven by the high voltage amplifiers (HVA, from OKOTech, Delft, The Netherlands) with an input range of 0–5 V, a DC voltage amplification of 80 and a -3 dB bandwidth of 1 kHz. The S-H WFS (OKOTech, Delft, The Netherlands) consists of 127 hexagonally distributed microlenses with a focal distance of 15 mm and pitch of 300 μm (see Fig. 1 (right) for the actuator-sensor layout). Each microlens provides a 2-dimensional measurement (i.e. horizontal and vertical movements of the spot) so that 254 sensor measurements are available in total. To make good use of the available sensor measurements but meanwhile reduce the computational complexity and improve the signal-to-noise ratio (SNR) of the system, 28 sensor measurements with high SNR are selected from the spots marked with $*$ for control. This over-parameterized sensor-actuator configuration is in accordance with many operational AO systems where there are more sensor measurements than actuators [20, 31, 34]. Vertical displacement from spot s1 is used for hysteresis identification in Section 5. The CCD camera (SVS340, SVS-VISTEK GmbH, Germany) has 640×480 square pixels of 7.4 μm and a maximum frame rate of 250 Hz. Via a frame grabber (Leonardo CL Full, ARVOO, The Netherlands), the image captured by the camera is transferred to the control computer (Dell Precision T7400, operated in openSUSE 10.3 with kernel 2.6.22). The controller is implemented in C code and integrated with the drivers of the camera and the digital-to-analog (D/A) card. The D/A card (PD2-AO-96/16, UEI, United States) has an output range of ± 10 V with 16-bit resolution.

3. Identification of the AO System

3.1. Strategy

To identify an accurate model of the AO system for controller design, the nonlinearity in the PDM, the high sampling rate in the WFS and the experimental conditions under which the data is collected should be considered.

Creep and hysteresis are two common nonlinearities in the PDM, originating from the piezo-actuators [9, 11, 37]. Creep can be considered as the drifting in the actuators which is observed when fixed DM deformation is required over extended periods of time, e.g. in the order of tens of seconds [9]. Since the time scale when creep takes effect is much longer than the sampling interval of the closed-loop AO system, creep can be neglected in closed-loop operation. Hysteresis can be considered as a static nonlinearity occurring at the input of the PDM, between the applied electrical field and the displacement of the piezo actuators [9]. Hysteresis in the PDM can be compensated by charge control [27], state initialization [23], local feedback linearization [4] or feedforward control [11, 37]. Among these approaches, feedforward control indicates a most cost-effective solution for hysteresis compensation (HC) in AO systems because it only requires an inverse hysteresis model of the piezo actuator instead of any hardware modification or extra samples in the control, but meanwhile provides efficient correction on hysteresis. Therefore feedforward control is used in our work to compensate for hysteresis in the PDM. The identification of the AO system can be summarized as follows.

- Compensate for the hysteresis in the PDM by feedforward control as shown in Fig. 3, where the hysteresis in each piezo actuator is compensated by the inverse hysteresis model identified from the measured hysteresis data. During the experiment, the PDM should be excited by slowly varying inputs with large amplitude such that the dynamics in the PDM can be neglected while the hysteresis is excited.
- After HC in the previous step, a dynamic model of the linear AO system (transfer from $u(k)$ to $y(k)$, denoted

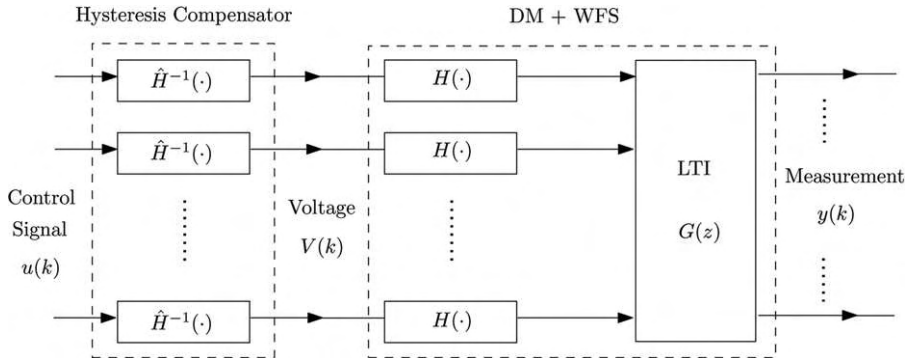

Fig. 3. Block diagram of the AO system, including the hysteresis compensator, DM and WFS.

as $G(z)$) can be identified at high sampling rate with a closed-loop subspace identification approach [5].

3.2. Hysteresis Compensation in the PDM

Referring to Fig. 3, the hysteresis compensator consists of m_u single-input single-output (SISO) inverse hysteresis models, one for each piezo actuator. The identification of the inverse hysteresis model involves parameterization of the model and parameter optimization. Concerning the model structure, Holman *et al.* [21] used separate polynomials to fit the hysteresis branches in the measurement data. Coleman-Hodgdon equations [6, 37] are also used to capture the hysteresis branches. Compared with these two, Preisach models [9, 11, 26] have more general structure and are very effective in capturing both the amplitude variations and non-symmetry in the hysteresis of the piezo-actuator. Therefore in our work Preisach inverse hysteresis model is applied.

The output of the Preisach model is calculated mainly in two steps: (1) determining the dominant local input extrema α and β; (2) evaluating the Preisach function $P(\alpha, \beta)$. The dominant local input extrema are determined by basic logic operations and updated with the input. The Preisach function $P(\alpha, \beta)$ is usually identified from the first-order reversal hysteresis curves and approximated e.g. by a look-up table [11] or a neural network [19].

3.3. Identification of the Linear AO System

After hysteresis compensation of the PDM, the transfer from the control input $u(k)$ to the sensor output $y(k)$ can be considered linear and a linear dynamic model can be identified for the controller design.

In general, the linear AO system can be represented in discrete state space form as [36]

$$x(k+1) = Ax(k) + Bu(k) + w(k), \tag{1}$$

$$y(k) = Cx(k) + \nu(k), \tag{2}$$

where $u(k) \in \mathbb{R}^{m_u}$, $y(k) \in \mathbb{R}^{m_y}$ and $x(k) \in \mathbb{R}^{m_x}$ are the input, output and state variable of the state space model at time instant k, respectively. $w(k) \in \mathbb{R}^{m_x}$ and $\nu(k) \in \mathbb{R}^{m_y}$ are the process noise and the measurement noise, respectively. $A \in \mathbb{R}^{m_x \times m_x}$, $B \in \mathbb{R}^{m_x \times m_u}$, $C \in \mathbb{R}^{m_y \times m_x}$ are the system matrices with m_x the order of the system. Here the direct feedthrough term is neglected, accounting for the inherent sample delay in the digital control system.

In the predictor-based subspace identification ($\text{PBSID}_{\text{opt}}$) algorithm [5], Eqs (1) and (2) are written in the innovation form as

$$\hat{x}(k+1) = A\hat{x}(k) + Bu(k) + K\epsilon(k), \tag{3}$$

$$y(k) = C\hat{x}(k) + \epsilon(k), \tag{4}$$

where $\hat{x}(k)$ is the one-step-ahead prediction of $x(k)$ and $K \in \mathbb{R}^{m_x \times m_y}$ is the Kalman gain. The innovation signal $\epsilon(k) \in \mathbb{R}^{m_y}$ is the one-step-ahead linear prediction error of $y(k)$, defined as $\epsilon(k) = y(k) - C\hat{x}(k)$. $A - KC$ is assumed to be stable and the system be controllable and observable.

The matrices A, B, C and K are identified in three steps: (1) the Markov parameters are estimated from the block Hankel matrices by solving a least squares problem; (2) the states of the system are estimated from Markov parameters and the Hankel matrices; (3) A, B, C and K are identified based on the Markov parameters, the Hankel matrices and the states of the system by solving two least squares problems. With the estimation of A, B and C available (denoted as $\hat{A}$, $\hat{B}$ and $\hat{C}$, respectively), the linear AO model can be constructed.

4. Model-Based Controller Design

The most common model-based controllers in closed-loop AO systems are LQG controllers [24, 25, 28] and H_2 optimal controllers [20]. The LQG controller is computed by solving two algebraic Riccati equations (ARE), one for Kalman gain design and the other for optimal state feedback. In the H_2 optimal controller [20], the feedback optimal controller design problem is converted to

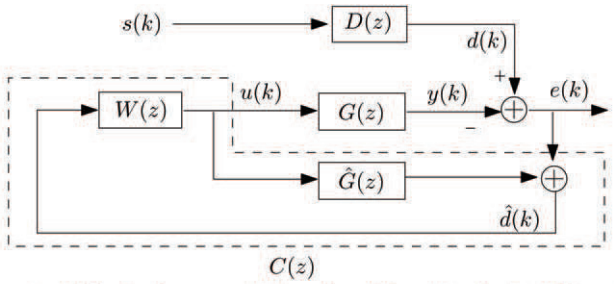

(a) Block diagram of the closed-loop feedback AO system

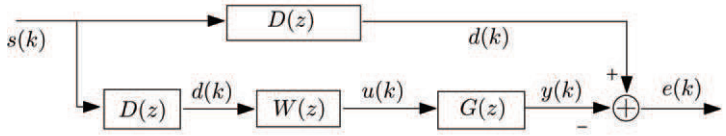

(b) Block diagram of the feedforward system

Fig. 4. The problem of finding optimal feedback control block $W(z)$ to minimize the cost function J in (a) is equivalent to finding the optimal feedforward controller $W(z)$ in (b).

a feedforward optimal controller design problem by the internal model control (IMC) approach. The feedforward optimal controller is then computed by applying the Causal Wiener Filter (CWF) theory. As proved by [14], the LQG and H_2 controller design methods result in the same input-output behavior of the controller and the same closed-loop performance, given the same disturbance model and AO model. Since the IMC approach used in H_2 optimal controller design allows to interpret the controller design in a pseudo open-loop manner that is commonly applied in standard AO control, the H_2 optimal controller design approach proposed in [20] is taken in our work.

Consider the block diagram of the closed-loop AO system in Fig. 4 (a), the transfer from $s(k)$ to disturbance $d(k)$ and from the control signal $u(k)$ to $y(k)$ are represented by asymptotically stable rational transfer functions $D(z)$ and $G(z)$, respectively. $C(z)$ is the controller structured by the IMC approach. The AO model $\hat{G}(z)$ is used to reconstruct the disturbance by removing the DM modulation from the residual error, i.e. $\hat{d}(k) = e(k) + \hat{y}(k)$. Here $\hat{d}(k)$ and $\hat{y}(k)$ are the estimation of disturbance and the DM modulation, respectively. With $\hat{d}(k)$ as input, the control signal $u(k)$ is generated by the control block $W(z)$ such that the cost function

$$J = \mathrm{tr}\mathbf{E}(e^T(k)e(k)) \tag{5}$$

is minimized, where $\mathrm{tr}(\cdot)$ is the trace operator and $\mathbf{E}(\cdot)$ is the stochastic expectation operator. The control block $W(z)$ and the controller $C(z)$ are related by

$$C(z) = (I - W(z)\hat{G}(z))^{-1}W(z). \tag{6}$$

The problem of finding optimal feedback control block $W(z)$ to minimize (5) in Fig. 4(a) is equivalent to finding the optimal feedforward controller $W(z)$ minimizing (5) in Fig. 4(b). Here it is assumed that $\hat{G}(z) = G(z)$ and $\hat{d}(k) = d(k)$. Because $s(k)$ is a white noise process with unit covariance, the cost function J in Fig. 4(b) can also be written as

$$J = \mathrm{tr}\mathbf{E}(e^T(k)e(k)) = \|D(z) - G(z)W(z)D(z)\|_2^2 \tag{7}$$

using Parseval's Theorem, where $\|\cdot\|_2$ represents the H_2 norm. The solution to this feedforward optimal controller design problem is given by the Causal Wiener Filter theory.

Lemma 1 (Causal Wiener Filter [14]): *Let $G(z)$ and $D(z)$ belong to the set of asymptotically stable rational transfer functions and assume that $G(z)$ and $D(z)$ do not lose rank $\forall|z| = 1$. Then the optimal feedforward controller $W(z)$ minimizing (7) is given by*

$$W(z) = G_o^{\dagger}(z)\left[G_i^*(z)D(z)D_{ci}^*(z)\right]_+ D_{co}^{\dagger}(z) \tag{8}$$

with $[\cdot]_+$ the causality operator and $(\cdot)^{\dagger}$ the left or right pseudo inverse. $G(z) = G_i(z)G_o(z)$ is an inner-outer factorization of $G(z)$, where $G_i(z)$ and $G_o(z)$ are asymptotically stable, $G_i^*(z)G_i(z) = I$ and $G_o(z)$ has a stable right inverse. $D(z) = D_{co}(z)D_{ci}(z)$ is an outer-inner factorization of $D(z)$, where $D_{co}(z)$ and $D_{ci}(z)$ are asymptotically stable, $D_{ci}(z)D_{ci}^*(z) = I$ and $D_{co}(z)$ has a stable left inverse.

Once the state-space realizations of $G(z)$ and $D(z)$ are given, the inner-outer factorization of $G(z)$ and the outer-inner factorization of $D(z)$ can be determined by solving two Riccati equations. If the disturbance $d(k)$ is an integrated white noise process, i.e. $D(z) = \frac{1}{1-z^{-1}}I$, and the

transfer from $u(k)$ to $y(k)$ is static except for a pure 1-sample delay (i.e. $G(z) = z^{-1}L$ where $L \in R^{m_y \times m_u}$ is the static gain with full column rank), then the analytical expression of the optimal controller can be derived from Eq. (6) and Eq. (8) as

$$W(z) = L^{\dagger}, \tag{9}$$

$$C(z) = \frac{1}{1 - z^{-1}} L^{\dagger}, \tag{10}$$

with

$$D_{ci}(z) = I, D_{co}(z) = \frac{1}{1 - z^{-1}}, \tag{11}$$

$$G_i(z) = z^{-1}U_1, G_o(z) = \Sigma_1 V^T, \tag{12}$$

$$L = U_1 \Sigma_1 V^T. \tag{13}$$

Eq. (13) is the singular value decomposition (SVD) of L in economy size, with Σ_1 a diagonal matrix containing m_u non-zero singular values. $L^{\dagger}$ is the pseudo-inverse of L such that $L^{\dagger}L = I$. It is worth noting that the optimal controller in Eq. (10) is just the conventional integrator-type controller with static gain $L^{\dagger}$ and pure integrator $\frac{1}{1-z^{-1}}$. This gives a nice physical interpretation of the controller. The static gain $L^{\dagger}$ is calculated by the CWF as in (9), which indicates that a static matrix projection is the optimal control action to minimize the residual error $e(k)$ in the feedforward scheme in Fig. 4(b), in case $d(k)$ is an integrated white noise process and DM is static. The integrator accounts for that only residual error $e(k)$ is available in closed-loop AO system instead of the disturbance itself.

To increase the robustness of the closed-loop AO system and prevent actuator saturation, two weighting parameters (denoted as $\rho_{in} \in \mathbb{R}$ and $\rho_{out} \in \mathbb{R}$) can be introduced in the controller design [14]. With ρ_{in} and ρ_{out}, the block $W(z)$ can be calculated as

$$W(z) = \tilde{G}_o^{\dagger}(z) \left[\tilde{G}_i^{*}(z) \bar{D}(z) \tilde{D}_{ci}^{*}(z) \right]_{+} \tilde{D}_{co}^{\dagger}(z), \tag{14}$$

where $\tilde{G}(z)$, $\tilde{D}(z)$ and $\bar{D}(z)$ are constructed as

$$\tilde{G}(z) = \begin{bmatrix} G(z) \\ \rho_{out} I_{m_u} \end{bmatrix}, \quad \tilde{D}(z) = \begin{bmatrix} D(z) & \rho_{in} I_{m_y} \end{bmatrix},$$

$$\bar{D}(z) = \begin{bmatrix} \tilde{D}(z) \\ 0_{m_u \times (m_y + m_s)} \end{bmatrix}. \tag{15}$$

$\tilde{G}(z) = \tilde{G}_i(z)\tilde{G}_o(z)$ is the inner-outer factorization of $\tilde{G}(z)$ and $\tilde{D}(z) = \tilde{D}_{co}(z)\tilde{D}_{ci}(z)$ is the outer-inner factorization of $\tilde{D}(z)$. I_{m_u} and I_{m_y} are the identity matrices with dimension m_u and m_y, respectively. ρ_{in} takes into account the measurement noise in $y(k)$. ρ_{out} balances the control effort $u(k)$ and the residual error $e(k)$. By increasing ρ_{in} and ρ_{out}, the measurement noise is accounted for more cautiously and control effort is reduced by the controller.

5. Experiments and Results

The experiments are devoted to hysteresis compensation of the PDM, identification of the linear AO system and performance evaluation of the closed-loop AO system with model-based controller. The experimental setup is the same as depicted in Fig. 1 with the number of inputs $m_u = 11$ and the number of outputs $m_y = 28$. The strategy in Section 3.1 is applied to obtain a linear dynamic model of the AO system. Controller design is based on Section 4.

The measurement noise in the AO setup is characterized from the WFS measurements while the disturbance is absent and the control signal is zero (i.e. $d(k) = 0$, $u(k) = 0$). 1000 WFS measurements have been collected at a sampling rate of 230 Hz. The standard deviation of the measurement noise is about 0.023 pixel. In the identification of the inverse hysteresis model, since the amplitude of the excitation signal is very large (about 30 pixels in the peak-to-peak value as shown in Fig. 6), the measurement noise is neglected. In the identification of the linear AO system, the effect of the measurement noise is incorporated by the $\text{PBSID}_{\text{opt}}$ closed-loop identification algorithm. In the model-based controller design, the influence of the measurement noise is accounted for by the parameter ρ_{in} as explained in Section 4. The value of ρ_{in} is tuned such that the best performance of the closed-loop AO system is achieved.

The timing of the closed-loop AO system is shown in Fig. 5. The delay from the exposure trigger to the control voltage generation (denoted as τ) mainly consists of: the exposure time t_e, the image transmission time $t_{m,1}$, the transmission time $t_{m,2}$ and the controller computational time t_c. Here $t_{m,2}$ also includes the image processing time. Based on the measured values of t_e, $t_{m,1}$, $t_{m,2}$ and t_c (shown in Fig. 5), the delay τ is about 7.5 ms. During hysteresis compensation, the sampling interval t_s is 50 ms, which is far more than τ and the settling time of the DM (about 3 ms); hence the transfer from $V(k)$ to $y(k)$ is static except for a pure 1-sample delay. During the AO model identification, the sampling interval t_s is 4.3 ms (230 Hz), the influence of $V(k)$ can only be sensed since Frame $k + 2$. The time interval between $V(k)$ and the exposure trigger $k + 2$ is about $2t_s - \tau = 1.1$ ms, which is less than the settling time of the DM. Therefore dynamics can be observed from $V(k)$ to $y(k)$ apart from a pure 1-sample delay.

5.1. Hysteresis Compensation

To get the hysteresis data of the piezo actuator, actuator 1 is excited by a saw tooth signal, denoted as $V_1(k)$, of which the local maxima slowly decreases in time while the local minima are constant. The period of the sawtooth signal is 5 s with the sampling rate of the WFS 20 Hz. The vertical displacement of spot s1 is recorded as $y_1(k)$ (the

t_s: sampling interval of the camera;
$t_e = 0.1$ ms: exposure time of the camera;
$t_{m,1} = 4.0$ ms: transmission time from the camera to the frame grabber;
$t_{m,2} = 3.4$ ms: transmission time from the frame grabber to CPU, including image processing;
$t_c = 35$ μs: controller computational time;
F_k: Frame k taken by the camera.

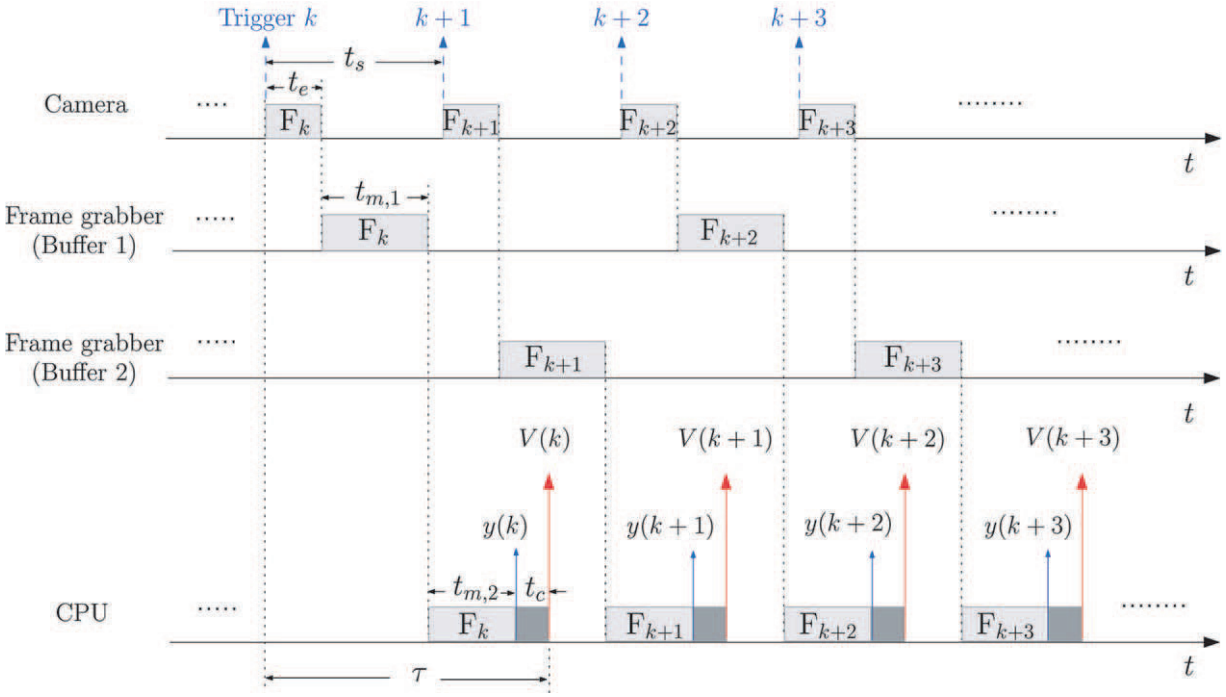

Fig. 5. Timing of the closed-loop AO system.

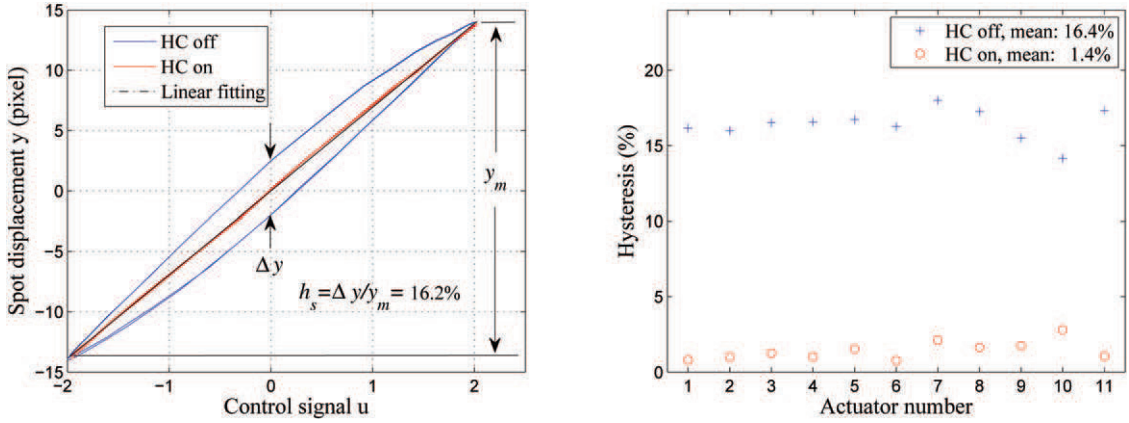

Fig. 6. Left: $(u_1(k), y_1(k))$ relationship with HC off (blue) and on (red); right: hysteresis in each actuator with HC off (cross) and on (circle).

pure 1-sample delay has been removed so that $V_1(k)$ and $y_1(k)$ are already synchronized).

A Preisach inverse hysteresis model is identified using $y_1(k)$ as input and $V_1(k)$ as output. The Preisach function $P(\alpha, \beta)$ is approximated by a two-layer feedforward neural network with eight neurons in the first layer and one neuron in the second layer. The neural network is trained by means of Levenberg-Marquardt (LM) backpropagation, using the MATLAB neural network toolbox [10]. Fig. 6 (left) shows the relationship between the control

signal $u_1(k)$ to actuator 1 and the measurement $y_1(k)$ when HC is off (solid, blue) and on (dashed, red). To quantify the hysteresis in the piezo actuator, a parameter h_s is defined as the ratio of the maximum possible output difference for any input (Δy) divided by the output range (y_m), i.e. $h_s = \Delta y / y_m$. After HC, h_s of actuator 1 has been reduced from 16.2% to 0.8% and the linearity of the input-output curve has been improved. This inverse hysteresis model is also used to compensate for hysteresis in all other actuators. The residual hysteresis in other actuators has been evaluated by exciting individual actuator one by one and measuring the displacement of the spot which gives best signal-to-noise ratio. The result is plotted in Fig. 6 (right), where the hysteresis of single piezo actuators has been reduced from 16.4% to 1.4% in average by HC.

To further validate the hysteresis compensator when all the piezo actuators are excited simultaneously, a spectral analysis based approach as described in [30] is used. In this approach, the PDM is excited by a multi-sine signal $u(k)$ where each channel of $u(k)$ consists of n_f harmonics at frequencies $(4i+1)f_0$, $i = 0, \cdots, n_f - 1$ with $f_0 \in \mathbb{R}$ the frequency resolution. If the transfer from $u(k)$ to $y(k)$ is linear, then $y(k)$ should only consists of harmonics at $(4i+1)f_0$; otherwise the power at $f \neq (4i+1)f_0$ can be used as a measure of the nonlinearity in the AO system. During the experiments, all the actuators in the DM are excited by the control signal $u(k)$ simultaneously, with 2000 time samples. The frequency resolution is set $f_0 = 0.01$ Hz and the sampling rate of the WFS is 20 Hz. Fig. 7 shows the spectrum averaged over all output channels in $y(k)$ with HC off (left) and on (right). The frequency components at $(4i+1)f_0$ are dominant in both plots, but the components at $(4i+3)f_0$ in Fig. 7 (left) is about one-magnitude above the noise level due to the nonlinearity in the AO system. After HC, these components at $(4i+3)f_0$ have been attenuated in Fig. 7 (right) to the same order as the noise, indicating significant improvement in the linearity of the AO system and validating the hysteresis compensator.

5.2. Identification of the Linear AO System

After hysteresis compensation, a linear dynamic model of the AO system is identified with the closed-loop subspace identification approach. The identification consists of the following steps:

1. Excite the AO system in open-loop with random control input $u_o(k)$ and record the measurement $y_o(k)$. The sampling rate of the WFS is 230 Hz. $\{u_o(k), y_o(k)\}$ consist of both the dynamics of the DM and a pure 1-sample delay. To get a static model of the AO system from $u_o(k)$ and $y_o(k)$, the measurement $y_o(k)$ is shifted by 2 time samples such that $\tilde{y}_o(k) = y_o(k+2)$, where $\tilde{y}_o(k)$ is the shifted output. A linear static model of the AO system, denoted as $\hat{L}$, is identified based on the data set $\{u_o(k), \tilde{y}_o(k)\}_{k=1}^{N}$ ($N = 2000$ is the length of the data set) by linear least squares fitting, i.e.

$$\hat{L} = \arg\min_{\hat{L}} \sum_{k=1}^{N} \|\tilde{y}_o(k) - \hat{L}u_o(k)\|_2^2. \tag{16}$$

   The accuracy of the static model $\hat{L}$ is evaluated by calculating the variance accounted for (VAF) of the model, which is defined as

$$\mathrm{VAF}(\hat{y}, \tilde{y}) = \left(1 - \frac{\mathrm{var}(\hat{y} - \tilde{y})}{\mathrm{var}(\tilde{y})}\right) \times 100\%. \tag{17}$$

   Here $\hat{y}$ is the estimation of $\tilde{y}$ and $\mathrm{var}(\tilde{y})$ is the variance of $\tilde{y}$. Static models have also been identified by shifting $y(k)$ by 1 or 3 time samples, but only shifting $y(k)$ by 2 time samples gives the highest VAF.
2. A conventional controller

$$C(z) = \frac{\mu}{1 - z^{-1}} (\hat{L}^T \hat{L} + \rho I)^{-1} \hat{L}^T, \tag{18}$$

   is implemented with $\mu \in \mathbb{R}$ and $\rho \in \mathbb{R}$ user-defined parameters. The closed-loop AO system with this conventional controller is then operational to reject the

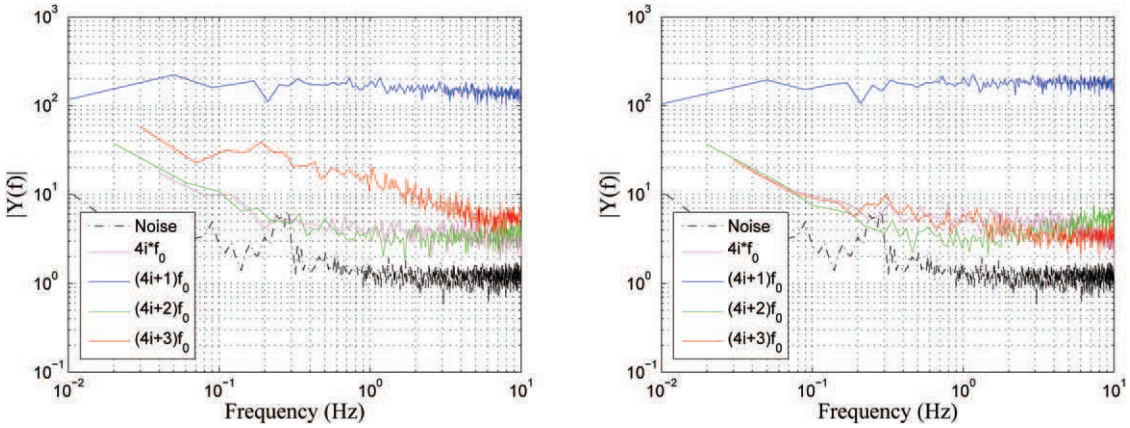

Fig. 7. Spectrum of the measurement $y(k)$ in case HC off (left) and on (right). $Y(f)$ is the Fourier transform of $y(k)$.

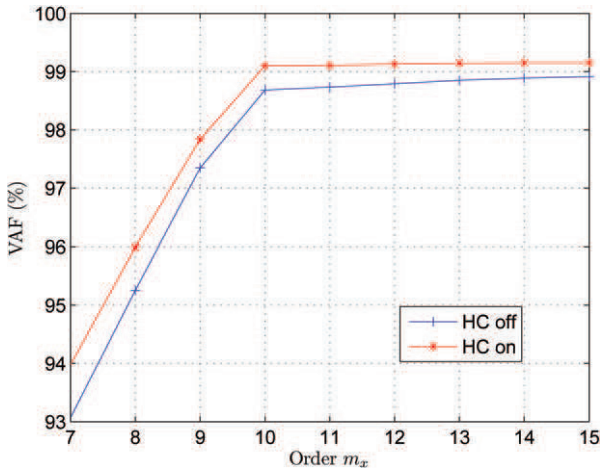

Fig. 8. VAF of the state-space model with respect to the order m_x, zoomed in for $m_x = 7, \ldots, 15$.

random disturbance $d(k)$ as in Fig. 2. The closed-loop experiments are carried out for two times. Each time a new set of $d(k)$ is generated. The control signal and the WFS measurement in these two closed-loop experiments are recorded as $\{u_{c1}(k), y_{c1}(k)\}_{k=1}^{N_c}$ and $\{u_{c2}(k), y_{c2}(k)\}_{k=1}^{N_c}$, respectively. The data length in these two experiments are $N_c = 2000$ and the sampling rate of the WFS is 230 Hz. $\mu = 0.2$ and $\rho = 2$ are taken in the controller to balance the stability and performance of the closed-loop AO system.

3. Considering that there is a pure 1-sample delay between $u_{c1}(k)$ and $y_{c1}(k)$, measurement $y_{c1}(k)$ is shifted by 1 time sample such that $\tilde{y}_{c1}(k) = y_{c1}(k+1)$, where $\tilde{y}_{c1}(k)$ is the shifted output. A set of dynamic models of the AO system are then identified from the data set $\{u_{c1}(k), \tilde{y}_{c1}(k)\}_{k=1}^{N_c}$, using the closed-loop subspace identification algorithm with the system order $m_x = 1, 2, \ldots, 20$. The VAF values of these dynamic models are evaluated and plotted in Fig. 8. There is significant difference in the VAF for $m_x \leq 10$, but an order higher than 10 gives very little improvement on the model accuracy. Therefore $m_x = 10$ is taken to balance the model accuracy and the model complexity. Apart from the numerical evaluation, a physical interpretation on this order selection is that since the DM surface has a free edge, the piston movement of the surface when all the actuators are deformed by the same amount can not be observed by WFS. Therefore effectively the DM only has 10 degrees-of-freedom.

   From the subspace identification algorithm, $\hat{A}$, $\hat{B}$ and $\hat{C}$ are obtained and the AO model from $u(k)$ to $y(k)$ is then obtained as $\hat{G}(z) = \hat{C}(zI - \hat{A})^{-1}\hat{B}z^{-1}$, where z^{-1} accounts for the shift in $\tilde{y}_{c1}(k)$. Because the disturbance $d(k)$ is introduced numerically in the controller instead of in the optical path, the response of the AO system $y(k)$ can be directly used for identification of the AO system. This corresponds to the calibration of the AO system in a telescope [5] where the atmospheric disturbance is absent and the AO system is subject to the excitation source.

4. The accuracy of the static model $\hat{L}$ and the dynamic model $\hat{G}(z)$ are evaluated with the fresh data set $\{u_{c2}(k), y_{c2}(k)\}_{k=1}^{N_c}$ according to the VAF of the models. In favor of the static model, the measurement $y_{c2}(k)$ is shifted by 2 time samples such that $\tilde{y}_{c2}(k) = y_{c2}(k+2)$ is used to validate $\hat{L}$. But in validating the dynamic model $\hat{G}(z)$, $y_{c2}(k)$ is used directly.

Table 1. VAF of the models of the AO system. The dynamic model with HC gives a significant improvement in the accuracy.

	Identification set		Validation set	
	Static model	Dynamic model	Static model	Dynamic model
HC off	78.2%	98.7%	72.0%	96.5%
HC on	82.1%	99.1%	79.8%	98.4%

Table 1 gives the VAF of the static model $\hat{L}$ and the dynamic model $\hat{G}(z)$ for the identification set and validation set, with HC off and on. The results are summarized as follows.

- Horizontally, the dynamic models result in higher VAF values than the static models in all cases. In the worst case, VAF of the dynamic model can still reach as high as 96.5% while only 82.1% can be reached with static model in best case.
- Vertically, the VAF values with HC on are higher than those with HC off in all cases. The difference is among 0.4% and 7.8%. Comparing the VAF in the identification set and the validation set, there is less variation in VAF with HC on than with HC off. This indicates that the uncertainty in the AO system has been reduced by HC.
- Comparing the VAF values in the top left corner (72.0%, in the validation set) and in the bottom right corner (98.4%), it can be concluded that the dynamic model with HC gives a significant improvement in the accuracy.

5.3. Performance of the Closed-Loop AO System

After the model of the AO system is identified, a controller is designed based on the identified model of the AO system and the disturbance model. The disturbance is assumed to be integrated white noise process in favor of the conventional controller, because it has been shown in Eq. (10) that the conventional controller is the optimal controller if

the DM is static and the disturbance is an integrated white noise process. In different applications, the disturbance may have different spatial or temporal characteristics other than an integrated white noise process. In that case, the filter $D(z)$ can be adapted according to the prior knowledge of the statistics of the disturbance (e.g. [7]), or be identified from the measurement data using a data-driven identification approach [20].

Experiments are carried out to evaluate the performance of the closed-loop AO system, with the disturbance $d(k)$ an integrated white noise process. The sampling rate of the closed-loop AO system is 230 Hz. The data length is $N = 1000$. The performance of the closed-loop AO system is evaluated in terms of the sum of the variance of the residual error (denoted as J_e), which is defined as

$$J_e = \frac{1}{N-1}\sum_{k=1}^{N}(e(k)-\bar{e})^T(e(k)-\bar{e}), \tag{19}$$

where $\bar{e}$ is the mean of $e(k)$ over N time samples. Comparison is made between four cases: conventional controller with HC off (A1) and HC on (A2), dynamic-model-based controller with HC off (B1) and HC on (B2). The parameters in all the controllers are tuned such that the best performance of each is achieved. Fig. 9 shows J_e achieved for different μ and ρ in the conventional controller and for different ρ_{in} and ρ_{out} in the proposed dynamic-model-based controller. It can be seen that the dynamic-model-based controllers (B1 and B2) result in less residual error than the conventional controller (A1 and A2). Minimal J_e is reduced from 13.8 (A1) to 10.4 (B1) and from 12.7 (A2) to 9.6 (B2). Hysteresis compensation improves the performance and performance robustness of the closed-loop AO system, either with the conventional controller or dynamic-model-based controller. Broader range of μ and ρ_{out}, e.g. $\mu = 0.5$ and $\rho_{out} = 0.4$, can be used in the controllers without severely deteriorating the performance. By combining hysteresis compensation and dynamic-model-based controller design, J_e has been reduced from 13.8 (A1) to 9.6 (B2), by about 30%.

Fig. 10 shows the transient response of the closed-loop AO system subject to static disturbance. The response is averaged over 20 experiments. In each experiment, a random static disturbance is applied since time $k = 0$. Due to the delay in the closed-loop AO system, the measurement is only influenced since $k = 2$. A1 and A2 require 4 time samples to reach about 10% of the initial error while B1 and B2 only take 3 time samples. The effect of hysteresis compensation can also be visualized, where a reduction of 0.13 is observed in the error variance at time sample 2 (from 0.34 in B1 to 0.21 in B2) and the oscillation at the 7*th* time sample in A1 is reduced significantly in A2.

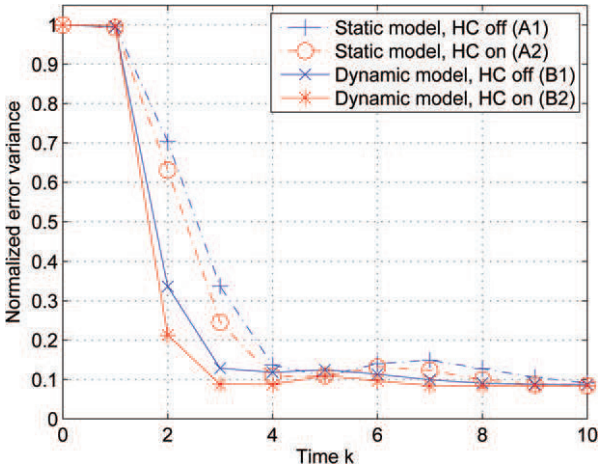

Fig. 10. Transient response of the closed-loop AO system subject to random static disturbance at a sampling rate of 230 Hz.

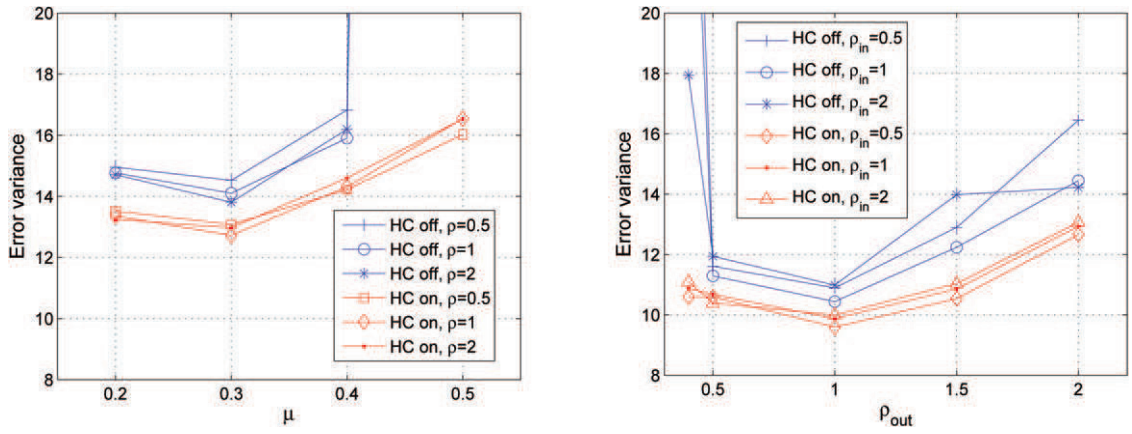

Fig. 9. Error variance J_e achieved for different μ and ρ in the conventional controller, and for different ρ_{in} and ρ_{out} in the proposed dynamic-model-based controller.

5.4. Computational Time

The controller computational time t_c (see Fig. 5) is important for real-time implementation of the closed-loop AO system. The computational load comes from the hysteresis compensator and the dynamic-model-based controller. Since the inverse hysteresis models in the hysteresis compensator have the same structure, the computational complexity of the hysteresis compensator is almost proportional to the number of actuators in the PDM. In our experiments, the computational time required by the hysteresis compensator is about 20 μs per sample (about 1.9 μs per actuator). The model-based controller is implemented in the state-space form with input dimension $m_y = 28$, output dimension $m_u = 11$ and an order of 21. The computational time for the dynamic-model-based controller is about 15 μs per sample, which results in a total computational time of $t_c = 20 + 15 = 35\,\mu s$. With conventional static-model-based controller and HC off, the computation takes about 5 μs. The additional 30 μs introduced by our dynamic-model-based controller with HC is negligible compared with the sampling interval of the closed-loop system ($t_s = 4.3$ ms), but a significant performance improvement can be achieved.

6. Conclusion

A model-based controller is designed and validated for a closed-loop AO system with PDM and high-sampling-rate WFS. The proposed controller consists of a hysteresis compensator reducing the hysteresis in the PDM and a linear model-based controller taking care of the linear dynamics in the closed-loop system.

The hysteresis in the piezo actuators is reduced from 16.4% to 1.4% in average by the hysteresis compensator. The identified dynamic AO model gives an improvement in VAF from 72.0% to 98.4%, compared to the conventional static AO model. The variance of the residual error of the closed-loop AO system has been reduced by 30% for integrated-white-noise disturbance. Transient response shows that the convergence speed and the robustness of the closed-loop AO system has been improved significantly.

Future work will focus on controller design based on the real disturbance and the AO system.

Acknowledgement

This work is supported by Delft Center for Mechatronics and Microsystems (DCMM). We would like to thank Mr. van Geest for implementing the control system, Ir. Houtzager for the identification algorithm, Dr. Soloviev and Dr. Loktev from OKOTech for their valuable comments. The constructive comments from anonymous reviewers are also appreciated.

References

1. Bifano T, Cornelissen S, Bierden P. MEMS deformable mirrors in astronomical adaptive optics. *Proceedings of 1st AO4ELT conference*, 2010, p. 06003.
2. Blain C, Conan R, Bradley C, Guyon O, Vogel C. Characterisation of the influence function non-additivities for a 1024-actuator MEMS deformable mirror. *Proceedings of 1st AO4ELT conference*, 2010, p. 06009.
3. Born M, Wolf E. *Principles of Optics: Electromagnetic Theory of Propagation, 7th ed.* Cambridge University Press, Cambridge, 1999.
4. Chang MP, Zadrozny A, Buscher DF, Dunlop CN, Robinson DJ. Hysteresis correction of a piezoelectrically actuated segmented mirror. *Proc SPIE* 1998; 3353: 864–871.
5. Chiuso A, Muradore R, Marchetti E. Dynamic calibration of adaptive optics systems: a system identification approach. *Proceedings of the 47th IEEE Conference on Decision and Control, CDC*, 2008, pp. 750–755.
6. Coleman B, Hodgdon M. A constitutive relation for rate-independent hysteresis in ferromagnetically soft material. *Int J Eng Sci* 1986; 24: 897–919.
7. Conan J-M, Rousset G, Madec PY. Wave-front temporal spectra in high-resolution imaging through turbulence. *J Opt Soc Am A* 1995; 12(7): 1559–1570.
8. Crépy B, Chaillot S, Conan JM, Cousty R, Delrez C, Dimmler M, Dournaux JL, De Zotti S, Gabriel E, Gasmi R, Grasser R, Hubin N, Jagourel P, Jochum L, Locre F, Madec P-Y, Morin P, Mueller M, Petit G, Petitgas D, Roland JJ, Sinquin JC, Vernet E. The M4 adaptive unit for the E-ELT. *Proceedings of 1st AO4ELT conference*, 2010, p. 06001.
9. Croft D, Shed G, Devasia S. Creep, hysteresis, and vibration compensation for piezoactuators: atomic force microscopy application. *ASME J Dyn Syst Meas and Control* 2001; 123: 35–43.
10. Demuth H, Beale M, Hagan M. *Neural Network Toolbox 5 User's Guide*. The MathWorks, Inc, 2007.
11. Dubra A, Massa J, Paterson C. Preisach classical and nonlinear modeling of hysteresis in piezoceramic deformable mirrors. *Opt Express* 2005; 13: 9062–9070.
12. Ellerbroek B. Optimizing closed-loop adaptive-optics performance with use of multiple control bandwidths. *J Opt Soc Am A* 1994; 11: 2871–2886.
13. Fedrigo E, Kasper M, Ivanescu L, Bonnet H. Real-time control of ESO adaptive optics systems. *Automatisierungstechnik* 2005; 53(10): 470–483.
14. Fraanje R. *Robust and Fast Schemes in Broadband Active Noise and Vibration Control*. PhD thesis, Enschede, 2004. Available at: http://doc.utwente.nl/41476/.
15. Gallieni D, Tintori M, Mantegazza M, Anaclerio E, Crimella L, Acerboni M, Biasi R, Angerer G, Andrigettoni M, Merler A, Veronese D, Carel J-L, Marque G, Molinari E, Tresoldi D, Toso G, Spanò P, Riva M, Riccardi A, Vernet E, Hubin N, Jochum L, Madec P, Dimmler M, Koch F. Voice-coil technology for the E-ELT M4 Adaptive Unit. *Proceedings of 1st AO4ELT conference*, 2010, p. 06002.
16. Gendron E, Léena P. Astronomical adaptive optics: I. modal control optimization. *Astronomy Astrophys* 1994; 291: 337–352.

17. Gevers M. Identification for control: from the early achievements to the revival of experiment design. *Eur J Control* 2005; 11: 1–18.
18. Hamelinck R, Rosielle N, Steinbuch M, Doelman N. Electromagnetic DM technology meets future AO demands. *Proceedings of 1st AO4ELT conference*, 2010; p. 06005.
19. Hinnen K, Fraanje R, Verhaegen M. The application of initial state correction in iterative learning control and the experiment validation on a piezoelectric tube scanner. *Proc Inst Mech Eng Part I – J Syst Control Eng* 2004; 218: 503–511.
20. Hinnen K, Verhaegen M, Doelman N. A data-driven $H2$-optimal control approach for adaptive optics. *IEEE Trans Control Syst Tech* 2008; 16: 381–395.
21. Holman A, Scholte P, Heerens W, Tunistra F. Analysis of piezo actuators in translation constructions. *Rev Sci Instrum* 1995; 66: 3208–3215.
22. Hubin N, Ellerbroek BL, Arsenault R, Clare RM, Dekany R, Gilles L, Kasper M, Herriot G, Le Louarn M, Marchetti E, Oberti S, Stoesz J, Veran JP, Vérinaud C. Adaptive optics for extremely large telescopes. *Proceedings of the International Astronomical Union* 1(Symposium S232), 2005, 60–85.
23. Kudryashov AV, Shmalhause VI. Semipassive bimorph exible mirrors for atmospheric adaptive optics applications. *Opt Eng* 1996; 35: 3064–3073.
24. Kulcsár C, Raynaud H-F, Petit C, Conan J-M, de Lesegno PV. Optimal control, observers and integrators in adaptive optics. *Opt Express* 2006; 14: 7464–7476.
25. Looze DP. Linear-quadratic-Gaussian control for adaptive optics systems using a hybrid model. *J Opt Soc Am A* 2009; 26: 1–9.
26. Mayergoyz ID. *Mathematical Models of Hysteresis and Their Applications*. Elsevier, Amsterdam, 2003.
27. Moheimani SOR, Fleming AJ. *Piezoelectric Transducers for Vibration Control and Damping*. Springer-Verlag, London, 2006.
28. Paschall R, Anderson D. Linear quadratic Gaussian control of a deformable mirror adaptive optics system with time-delayed measurements. *Appl Opt* 1993; 32: 6347–6358.
29. Petit C, Conan J-M, Kulcsár C, Raynaud H-F, Fusco T, Montri J, Rabaud D. Optimal control for multi-conjugate adaptive optics. *Comptes Rendus Physique* 2005; 6(10): 1059–1069.
30. Pintelon R, Schoukens J. *System Identification: A Frequency Domain Approach*. IEEE Press, New York, 2001.
31. Roddier F. *Adaptive Optics in Astronomy*. Cambridge University Press, Cambridge, 1999.
32. Roux BL, Conan J-M, Kulcsár C, Raynaud H-F, Mugnier L, Fusco T. Optimal control law for classical and multiconjugate adaptive optics. *J Opt Soc Am A* 2004; 21: 1261–1276.
33. Thompson SJ, Doel P, Brooks D, Strangwood M. A 1-metre Ni coated CFRP demonstrator for large deformable mirrors. *Proceedings of 1st AO4ELT conference*, 2010, p. 06007.
34. Tyson R. *Principle of Adaptive Optics*. Academic Press, Boston, 1998.
35. Vdovin G, Sarro PM. Flexible mirror micromachined in silicon. *Appl Opt* 1995; 34(16): 2968–2972.
36. Verhaegen M, Verdult V. *Filtering and System Identification: A Least Squares Approach*. Cambridge University Press, Cambridge, 2007.
37. Yang Q, Ftaclas C, Chun M, Toomey D. Hysteresis correction in the curvature adaptive optics system. *J Opt Soc Am A* 2005; 22: 142–147.